International Journal of ISSI, Vol. 13 (2016), No. 1, pp. 27-38

The Effects of Inhomogeneous Mechanical Properties of the Ferrite Phase on Dual Phase Steel's Behavior

S. Zarei [1] , R. Jafari Nedoushan [2*]

Department of Mechanical Engineering, Isfahan University of Technology, Isfahan 84156-83111, Iran

Abstract

The microstructure of dual phase steels can be considered as a matrix of ferrite phase reinforced by martensite particles. Recent measurements show that the mechanical properties of the ferrite phase are changed with the distance from the martensite grains. In this paper, a new method has been proposed to consider this phenomenon in finite element modeling of dual phase steels microstructure. In this method, ferrite mechanical properties were imported to the model as a continuous function of the distance from martensite boundary. A unit cell model of dual phase steel was constructed based on the experimental measurements. The tensile test was simulated in both cases of considering the ferrite phase as the homogeneous and inhomogeneous matrix. It was observed that by considering the ferrite phase inhomogeneity, the model could predict macro stress precisely. Considering the ferrite phase inhomogeneity also led to the better prediction of shear band formation in the unit cell, as compared to the other model. A different stress distribution prediction was also observed in these two models and ferrite phase maximum stress was higher when inhomogeneity was included. These observations could be crucial in the investigation of dual phase steels damage. It was observed that martensite volume fraction and the grain size had a stronger effect on the model with the inhomogeneous ferrite phase.

Keywords: Dual phase steels; Finite element microstructural modeling; Ferrite phase inhomogeneity.

1. Introduction

Industrial applications of sheet metal forming require materials with high plastic deformation potential and high strength. Dual phase (DP) steels are very interesting for lightweight constructions because they combine these two requirements. DP steels consisting of hard martensite islands within a ferrite matrix have received considerable attention due to their continuous yielding behavior, high work hardening rate and ductility [1)].

Stress–strain response of multiphase materials similar to DP steel depends on the elastic–plastic behavior of all ingredient phases. In recent years, computational modeling has been successfully established to study the material's mechanical behaviors at the microstructure level [2)].

** Corresponding author*
Tell: +98 31 339 15277
Email: rjafari@cc.iut.ac.ir
Address: Department of Mechanical Engineering, Isfahan University of Technology, Isfahan, Iran. P.O. Box: 84156-83111
1. M.Sc.
2. Assistant Professor

Micromechanical simulations were conducted on DP steels idealized to be spherical inclusions of martensite embedded in the ferrite matrix by Al-Abbasi and Nemes [3-5)]. Khaleel et al. [6-9)] used the classical plasticity theory on unit cell (UC) models generated from the real scanning electron microscope. It was concluded from their works that the failure of DP steels was driven by softening and plastic strain localization rather than nucleation, coalescence, and growth of voids.

Ramazani et al. [10-15)] have made a significant effort to understand the behavior of DP steels through UC computational modeling. Damage in the dual phase steel was investigated using digital image correlation in conjunction with microstructure simulation 16). Multiscale approach has also been used to model the dual-phase steels behavior [17, 18)]. Furthermore, in several works, various UC-based microstructures were used to simulate the plastic flow behavior of DP steels [1, 19-25)].

Recent measurements have shown that the properties of the ferrite phase are changed with the distance from the martensite grains [1, 14, 26)]. These measurements have revealed that the grains of the ferrite phase are harder in the vicinity of martensite grains. As a consequence of this local hardening effect, the ferrite phase has to be considered as an inhomogeneous matrix in

modeling DP steels.

Kadkhodapour et al. [1] used a UC model consisting of only a single martensite grain and a single ferrite grain to which varying properties were assigned by partitioning. This model, for the first time, led to a good agreement with the experimental observations of the mechanical stress–strain behavior. Some other simulations considered the ferrite phase as two distinct regions [12, 14, 27, 28]. The one adjacent to the martensite phase is addressed as the boundary region that has harder properties.

Abid et al. [28] created virtual random representative volume elements (RVEs) depicting the actual and highly equiaxed heterogeneous microstructure of DP steels. They used some experimentally measured thickness for the boundary region. Sirinakorn et al. [27] investigated deformation and fracture behavior of DP steel by means of some kind of microstructure-based finite element modeling. They considered the effect of ferrite inhomogeneity by taking into account transformation-induced geometrically necessary dislocations in the RVEs. Hosseini-Toudeshky et al. [26] considered ferrite and martensite interface debonding to predict the stress–strain behavior of DP steel using a finite element micromechanical approach. Interface elements based on the cohesive zone modeling were also used for the consideration of damage or debonding on the ferrite and martensite interfaces. Ramazani et al. [12, 14] predicted the work-hardening behavior of DP steel by focusing on the effect of transformation-induced geometrically necessary dislocations, showing the effect of the ferrite-martensite boundary (FMB).

All of the above-mentioned works divide the ferrite phase into two distinct regions, and do not implement the continuous change of ferrite phase properties [1]. In the current paper, ferrite mechanical properties were imported to the microstructure UC model of DP steel as the continuous function of the distance from FMB. The tensile test was simulated in both cases of considering the ferrite phase as the homogeneous and inhomogeneous matrix. The results of these models, including predicted micro and macro-stress and strain, were compared with each other and with the experimental data.

In the remaining part of this paper, first, the creation of UC geometry and the assigned constitutive laws are explained, and then the results of different models are investigated.

2. Microstructural Modeling

The finite element method was used to analyze a UC of the ferrite matrix and martensite grains. Perfect bonding along the ferrite and martensite boundaries was assumed.

2.1. Micromechanical geometry

The UC geometry was created by python scripting in commercial finite element code Abaqus. The created model was in the two dimensional space with the plane strain assumption, resulting in a higher degree of strain localization [14, 29], but in our simulations, all of the cases were investigated at the same condition, and the results were compared.

Model's characteristics, such as the martensite grain size and martensite volume fraction, were adopted on the real material [1]. The values of these parameters are shown in Table 1, with the elastic properties of each phase. Shapes and positions of the martensite grains were randomly created by python scripting. For this purpose, first, the center of each martensite grain was randomly chosen; then, a hexagon with random but a desired average grain size was constructed around the center. After calculating the positions of six vertexes, the hexagon interference with other created grains was checked. If there were no interference, the grain would be added to the model. The grain could be added to the model until the desired martensite volume fraction would be obtained. Fig. 1 shows a typical real microstructure of DP steel with the bright ferrite phase and dark martensite grains.

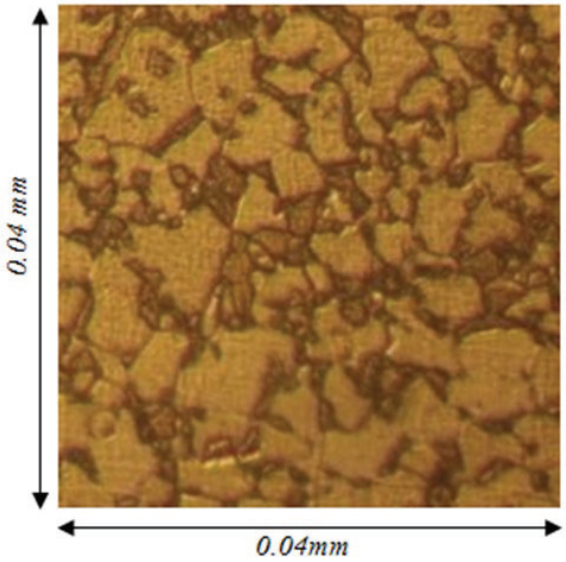

Fig.1. Real microstructure of DP steel with the bright ferrite phase and dark martensite grains.

Two different random models were generated to show the independency of the results on the initial UC model. Figs. 2 and 3 show these two models. As can be seen, martensite grains positions and shapes were different, but martensite volume fraction and average grain size were identical for both models.

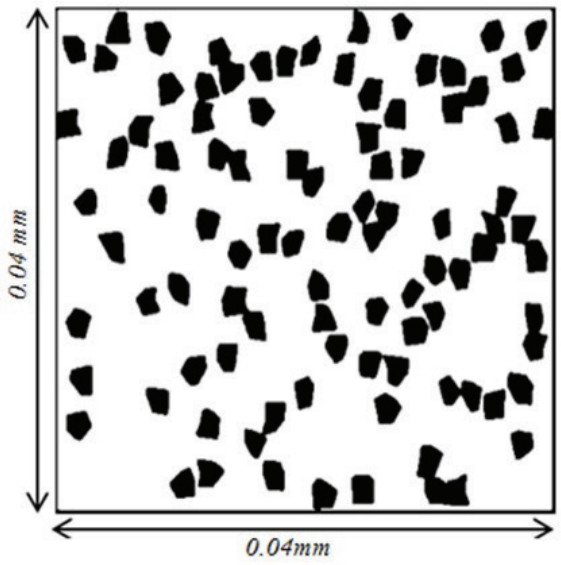

Fig. 2. First randomly created UC model with the white ferrite phase and black martensite grains.

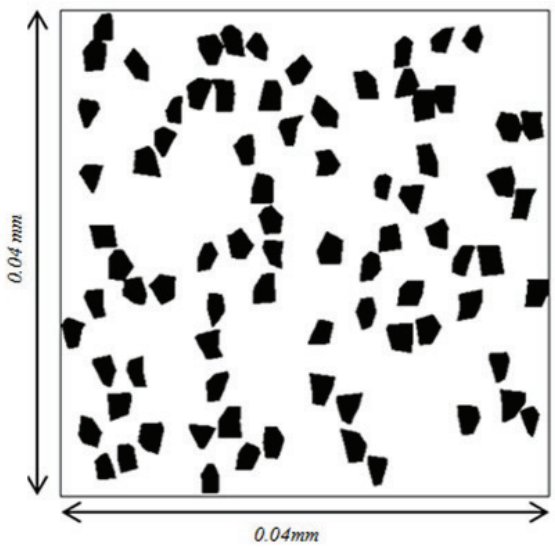

Fig. 3. The second randomly created UC model with the white ferrite phase and black martensite grains.

Table 1. Properties of ferrite and martensite phase.

Phase	Property	Value
Ferrite	E [29)]	220000(MPa)
	ν [29)]	0.3
Martensite	E [29)]	195000(MPa)
	ν [29)]	0.3
	volume fraction [1)]	0.15
	average grain size [1)]	2(μm)

2.2. Constitutive equations of phases

Von Mises criterion with isotropic hardening law was used to explain the constitutive behaviors of each phase. Martensite phase was assumed as a homogenous material whose hardening behavior is shown in Fig.4. The ferrite phase stress-strain curve could be obtained from the curve of this figure when multiplied by a coefficient expressing the distance from FMBs.

2.3. Dependency of ferrite phase behavior on the distance from FMB

Experimental observations have shown that ferrite phase has a harder behavior near FMB. Fig. 5 shows the results of nano-hardness tests conducted by Kadkhodapour et al. [1)] on the ferrite phase. As shown, the highest hardness was near the FMB, and it could be reduced to a definite value far from the boundary. Since yield and the ultimate stress of a material are proportional to its hardness [31, 32)] it could be concluded that these parameters also had the same dependency on the distance from FMB. Therefore, a function was fitted on the curve shown in Fig.5, and this function could be used to explain the hardening behavior of each point inside the ferrite phase.

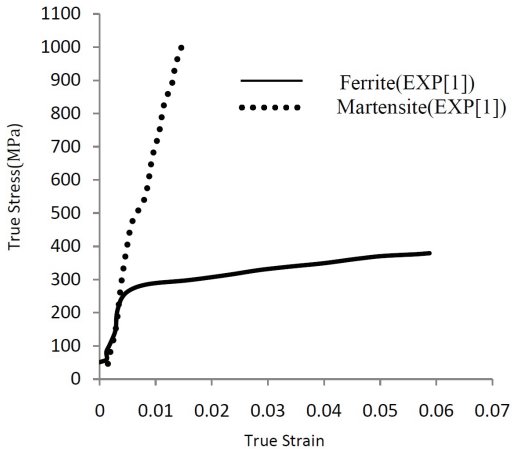

Fig. 4. Hardening behavior of ferrite and martensite phases [1)].

The fitting function has the following form:

$$f(x) = a \times d^{\,b} + c \qquad \text{(Eq. 1)}$$

, where d is the distance from FMB. The values of the above function›s coefficients are listed in Table 2. The fitted function is compared with the experimental measurement in Fig. 5.

Table 2. Values of fitting function's coefficients

Coefficient	a	b	c
Value	-2.187×10^{5}	0.003278	2.189×10^{5}

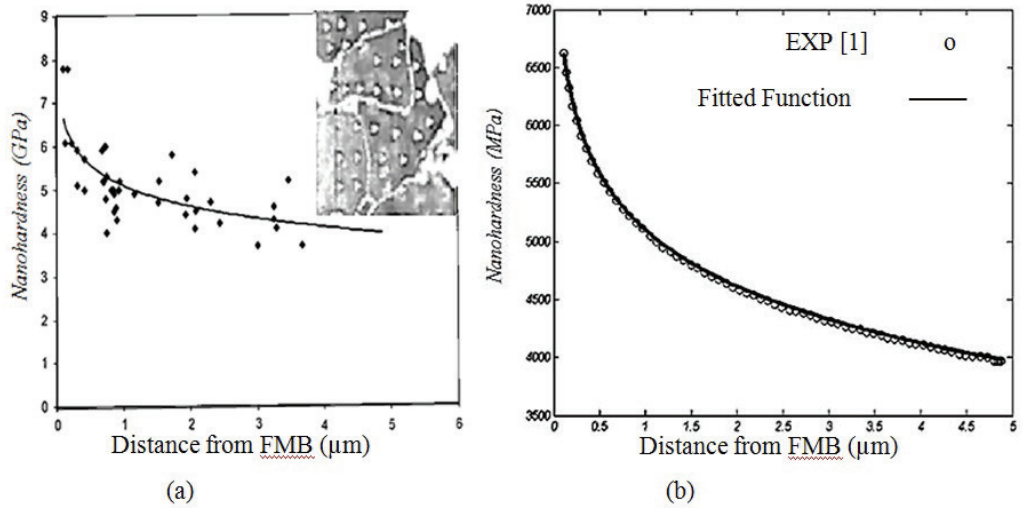

Fig. 5. (a) Results of the nano-indentation test of Kadkhodapour et al [1], and (b) Fitted function.

The hardening behavior shown in Fig. 4 was used for the integration points of the ferrite phase, but a coefficient derived from Fig. 5 could be multiplied by the stresses.

2.4. Implementation of ferrite inhomogeneity in the finite element method

To implement the inhomogeneity of ferrite phase in finite element modeling, the behavior of each integration point was defined by a user subroutine UMAT based on the distance from FMB. In this subroutine, coordinates of integration points are available as an argument. At first, the distance from FMB was calculated by this coordinate and the position of the nearest boundary line was extracted from the python code. Then, the hardening curve was constructed by the hardening curve of Fig. 5, and this calculated the distance. Finally, von Mises criterion and isotropic hardening law were used to explain the material behavior of this point.
The next section gives more details regarding the implementation of the von Mises criterion in the UMAT subroutine.

2.5. Implementation of Mises yield criterion

In this section, a brief description of the relationships used to implement Mises criterion, using the UMAT subroutine, is brought. Mises yield function, considering isotropic hardening, can be written as follows:

$$\sqrt{\frac{3}{2}S_{ij}S_{ij}} - \sigma_y\left(\bar{\varepsilon}^{pl}\right) = 0 \qquad \text{(Eq. 2)}$$

, where σ_y is the yield stress, $\bar{\varepsilon}^{pl}$ is the equivalent plastic strain, and S_{ij} is the deviatoric stress tensor:

$$S_{ij} = \sigma_{ij} - \frac{1}{3}\delta_{ij}\sigma_{kk} \qquad \text{(Eq. 3)}$$

, where σ_{ij} is the total stress tensor, and δ_{ij} is Kronecker delta. Equivalent plastic strain is defined as:

$$\bar{\varepsilon}^{pl} = \int_0^t \dot{\bar{\varepsilon}}^{pl}\, dt \qquad \text{(Eq. 4)}$$

$$\dot{\bar{\varepsilon}}^{pl} = \sqrt{\frac{2}{3}\dot{\varepsilon}_{ij}^{pl}\dot{\varepsilon}_{ij}^{pl}} \qquad \text{(Eq. 5)}$$

, where $\dot{\bar{\varepsilon}}^{pl}$ is the equivalent plastic strain rate, and $\dot{\varepsilon}_{ij}^{pl}$ is the plastic strain rate tensor that can be calculated from the plastic flow rule:

$$\dot{\varepsilon}_{ij}^{pl} = \frac{3}{2}\frac{S_{ij}}{\sigma_y}\dot{\bar{\varepsilon}}^{pl} \qquad \text{(Eq. 6)}$$

To implement the above equations in the FEM software, at first, deviatoric stress tensor and equivalent stress are calculated based on elastic prediction as follows:

$$S_{ij}^{tr} = S_{ij}^{0} + 2\mu\Delta e_{ij} \quad \text{(Eq. 7)}$$

$$\Delta e_{ij} = e_{ij} - e_{ij}^{0} \quad \text{(Eq. 8)}$$

$$\bar{\sigma}^{tr} = \sqrt{\frac{3}{2} S_{ij}^{tr} S_{ij}^{tr}} \quad \text{(Eq. 9)}$$

,where S_{ij}^{tr} is trial deviatoric stress tensor from the assumed elastic prediction, S_{ij}^{0} is the initial deviatoric stress tensor, μ is the shear modulus, e_{ij} and e_{ij}^{0} refer to current and initial deviatoric strain tensor, and $\bar{\sigma}^{tr}$ is the equivalent stress from elastic guess. After some manipulation, we can reduce the problem to a single equation in terms of the incremental equivalent plastic strain:

$$\bar{\sigma}^{tr} - 3\mu\Delta\bar{\varepsilon}^{pl} = \sigma_y\left(\bar{\varepsilon}^{pl}\right) \quad \text{(Eq. 10)}$$

This equation is solved by Newton's method. Then following equations are used to update the stress and plastic strain:

$$\sigma_{ij} = \eta_{ij}\sigma_y + \frac{1}{3}\delta_{ij}\sigma_{kk}^{tr} \quad \text{(Eq. 11)}$$

$$\Delta\varepsilon_{ij}^{pl} = \frac{3}{2}\eta_{ij}\Delta\bar{\varepsilon}^{pl} \quad \text{(Eq. 12)}$$

, where η_{ij} is defined as follows:

$$\eta_{ij} = S_{ij}^{tr} / \bar{\sigma}^{tr} \quad \text{(Eq. 13)}$$

2.6. Boundary conditions and discretization

The UC model is subjected to boundary loading, approximating uniaxial tension. As can be seen in Fig. 6, symmetry conditions were applied on left and bottom sides and constraint equation was applied to the nodes on the top line to have equal displacements in the y-direction at all nodes.
The geometry was meshed using about 3600 linear, reduced integration quadrilateral elements (Fig. 7). In order to do the mesh study, different resolutions of mesh were also investigated, as discussed later.

3. Results and discussion

At first, three different UC models were investigated, and the results were compared with each other and with the available experimental data. These models are listed below:
Model I: The UC model shown in Fig. 2 without considering the ferrite phase inhomogeneity
Model II: The UC model shown in Fig. 2 by applying the ferrite phase inhomogeneity
Model III: The UC model shown in Fig. 3 by applying the ferrite phase inhomogeneity

Comparing models I and II can show the effects of considering the ferrite phase inhomogeneity while models II and III only differ in the initial randomly created microstructure, and they can be used to investigate the initial microstructure dependency. In the following section, first, the mesh dependency of the model is investigated, and then the effects of various parameters are discussed.

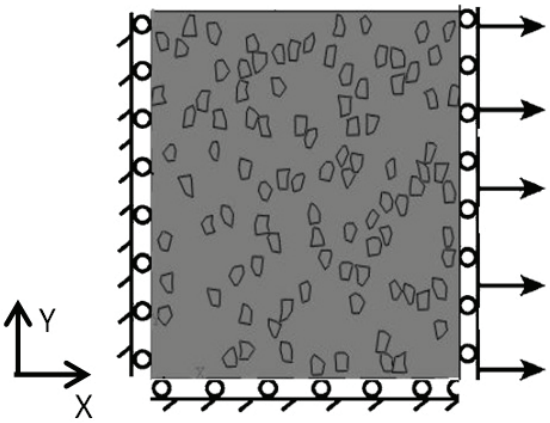

Fig. 6. Applying tensile loading on the boundaries of the UC model.

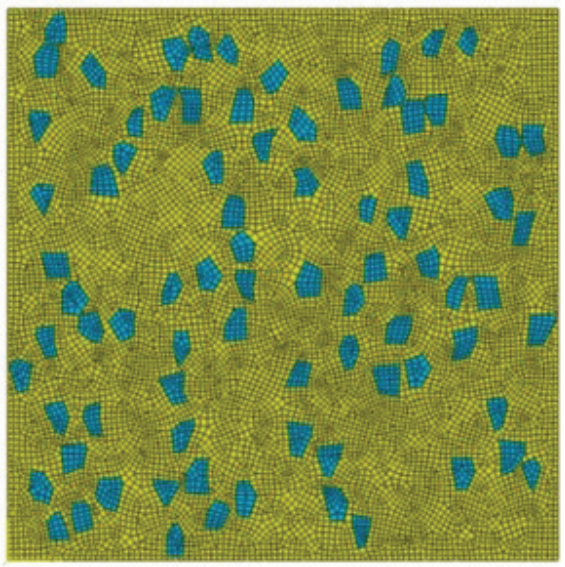

Fig. 7. Discretized model used for finite element modeling with the martensite phase in blue and ferrite matrix in the yellow color.

3.1. Mesh size effect

Mesh-size dependency is a well-known difficulty in the modeling of microstructures using the finite element method. In this section, the obtained results for micromechanical analyses with three different meshes are discussed. The predicted stress–strain

behaviors with different mesh resolutions were compared with each other in model II (Fig. 8). As can be seen from this figure, the predicted stress was mesh independent for mesh sizes less than 0.7µm. A similar result was also seen for other models. Therefore, it could concluded that if mesh size were less than 0.7 µm, the model would be mesh independent. A larger mesh size could not be used due to the convergence difficulty.

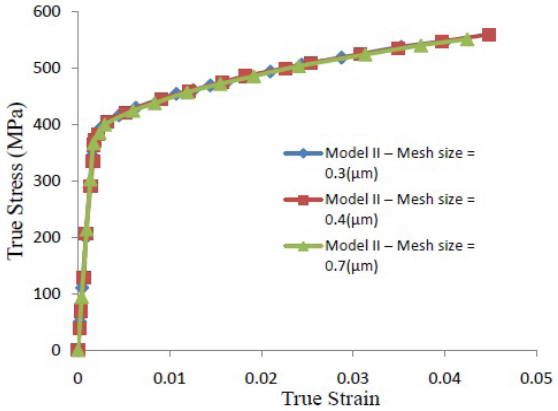

Fig. 8. The stress-strain curve for the DP steel behavior in different element sizes.

3.2. Stress distribution

Fig. 9 shows calculated von Mises stress distribution at the nominal strain of 0.05 by model I. As expected, martensite phase bore a higher stress due to its harder property. In the ferrite phase, there was a stress gradient depending on the distance from FMB. In this case, as distance from FMB was increased, the stress was decreased. To evaluate this change, calculated stresses in the ferrite phase for points near the FMBs and at points located in the center of the ferrite phase were compared. An average increase of 30 percent in von Mises stress was observed as we moved towards FMB.

At the first step, the provided subroutine which calculated the distance from FMBs was checked. This subroutine was used in models II and III to calculate the parameter d in Eq. (1), and then the stress coefficient was calculated by this equation.

To validate the method in which the distance from FMBs was calculated, this distance and the stress coefficient derived from Eq. (1) are shown in Fig. 10 at the beginning of the solution. The calculated distance should be zero on the FMBs, and the value should be equal to the distance from the nearest boundary on every other point. These expectations are seen in Fig. 10 a. In figure 10 b, the value of the stress coefficient should be the highest on the FMBs and reduced in points far from the FMBs.

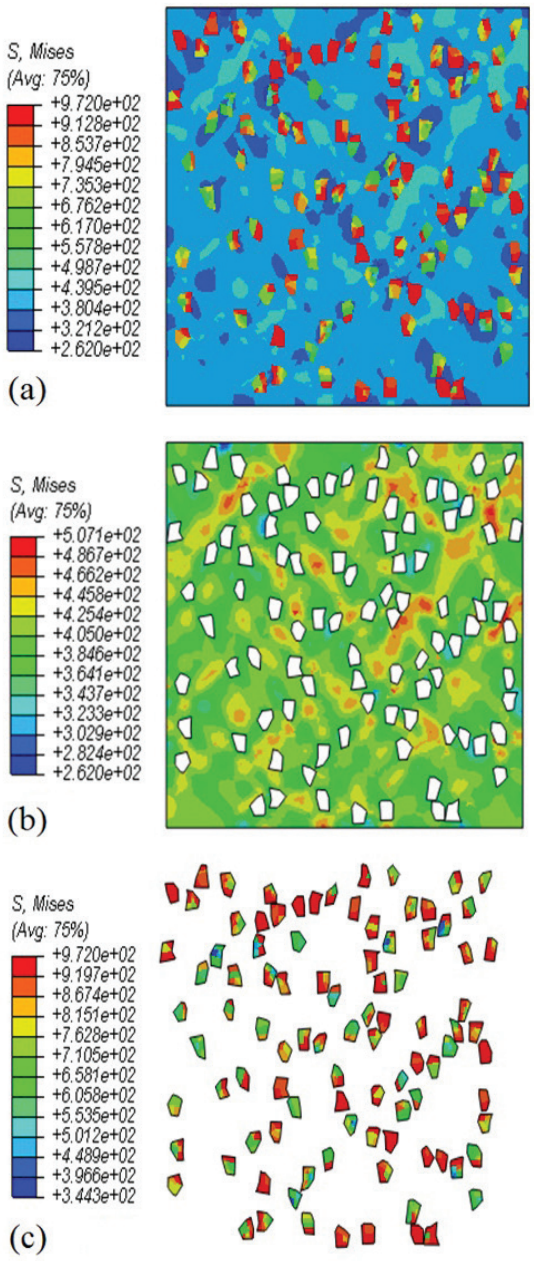

Fig. 9. Calculated von Mises stress distribution by model I (with the homogeneous ferrite phase) after 5% nominal strain (a) whole model, (b) ferrite phase, and (c) martensite islands.

Predicted von Mises stress distribution at the strain of 0.05 by model II is shown in Fig. 11. As in the previous model, martensite phase bore a higher stress, and in the ferrite phase, there was a stress gradient. In this case, as the distance from FMB was decreased, the stress was increased more than that predicted by model I (the average increase of 60 percent).

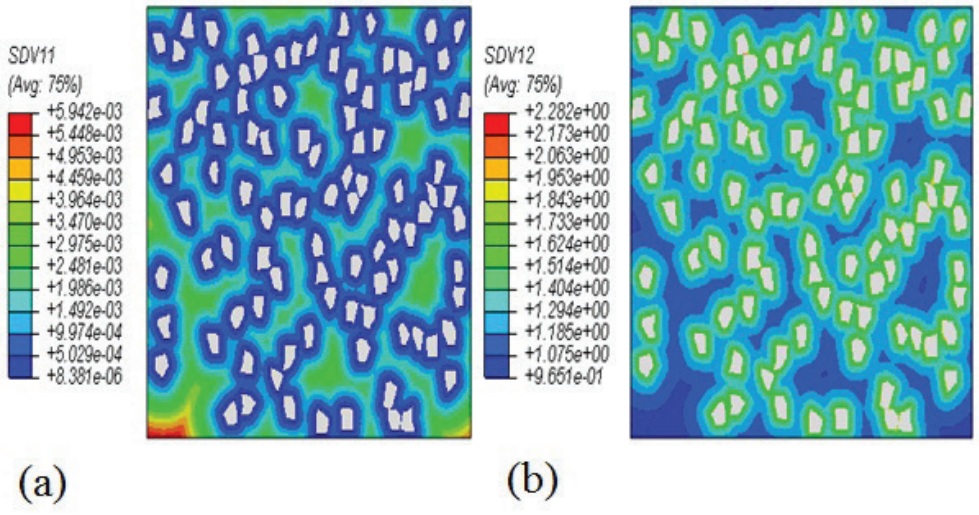

Fig. 10. (a) Calculated distance from FMB, and (b) Calculated stress coefficient at the beginning of the solutions.

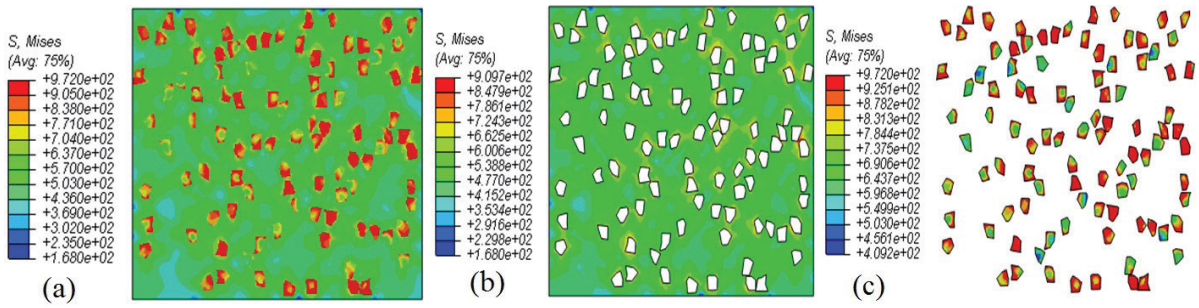

Fig. 11. Calculated von Mises stress distribution by model II (with the Nonhomogeneous ferrite phase) after 5% nominal strain (a) whole model, (b) ferrite phase, and (c) martensite islands.

3.3. Strain distribution and shear bands formation

Figs 12-14 show the predicted effective plastic strain distribution in the three mentioned models. In both models, II and III, shear bands were formed earlier than that predicted in model I. While shear bands were obvious in models II and III, in model I, there was no band formation. This observation showed the significance of the inhomogeneity of ferrite phase in the stress-strain behavior of the UC model.

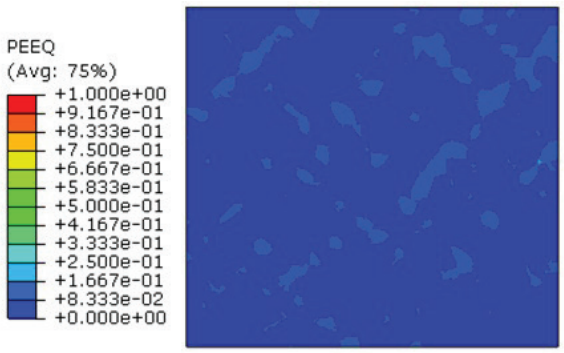

Fig. 12. The predicted effective plastic strain in model I after 10% nominal strain.

As shown in Fig. 15, by increasing the applied macro strain, shear bands could be more obvious. The shear band came through martensite particles which were close together, as previously reported by Schellekens et al. [30]. Plastic strain localization occurred in the shear band at an angle near 45 degrees between the shear band and loading direction, as previously observed in the results obtained by Kadkhodapour et al.

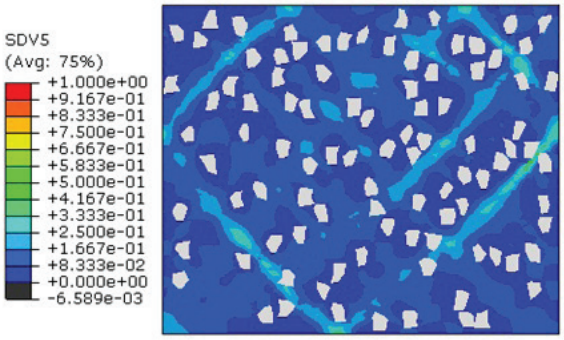

Fig. 13. The predicted effective plastic strain in model II after 10% nominal strain.

3.4. Predicted macro stress

Fig. 16 shows the predicted macro stress of the three mentioned micro models and compares their

results with the experimental curve [1]. The first model predicted a stress less than the real behavior. This was due to the fact that by considering a homogenous ferrite phase, the increase in ferrite phase strength could be neglected, and the macro behavior was softer than the real material. Models II and III predicted a stress-strain curve close together, showing that the results did not depend on the initial randomly-created microstructure.

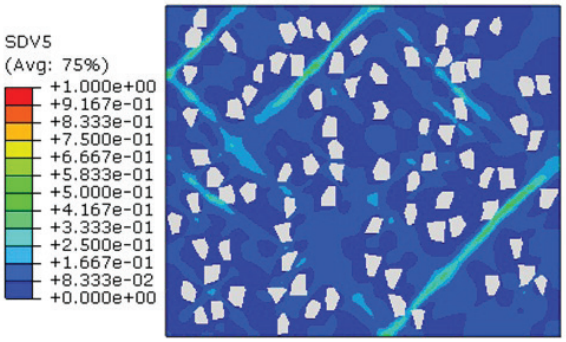

Fig. 14. The predicted effective plastic strain in model III after 10% nominal strain.

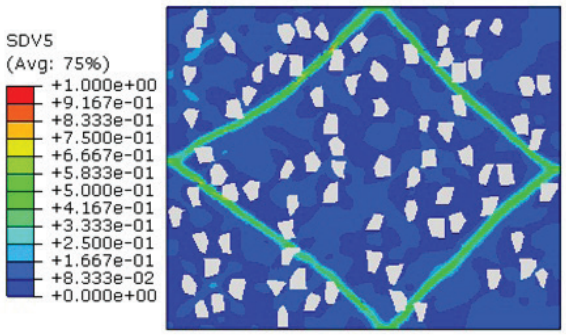

Fig. 15. The predicted effective plastic strain in model III after 15% nominal strain.

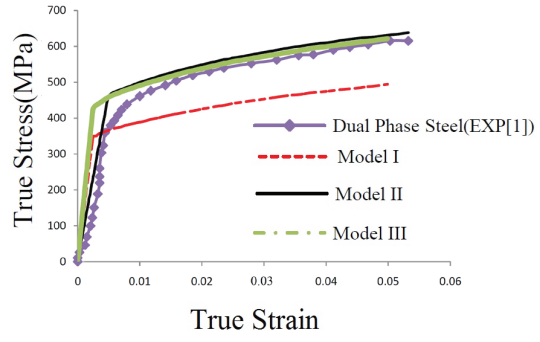

Fig. 16. The predicted stress-strain curve by the current models in comparison to the experimental data [1].

The predicted stress by models II and III was closer to the experimental data, as compared with the model I, again showing the importance of the ferrite phase inhomogeneity. It is worth mentioning that modeling of the unit cell in the three-dimensional space could slightly change all the curves [15], but would not change this result.

3.5. Effects of martensite volume fraction

In this section, the effects of martensite volume fraction on the mechanical behavior of DP steels for both homogenous and inhomogeneous ferrite phase models were compared. Experimental results from the literature suggest that increasing the martensite volume fraction enhances the ultimate tensile strength, while the ultimate elongation is decreased [33-36]. To gain more insight into this phenomenon, DP steels microstructures with 15, 20 and 30 percent of martensite were created. These generated microstructures are shown in Figs. 2 and 17.

The global response of these different microstructures can be seen in Fig. 18. It was expected that the tensile strength would be increased with increasing martensite volume fraction, but the notable observation in this figure was the difference between models considering ferrite inhomogeneity and those considering the homogenous ferrite phase. A larger rise in stress with increasing martensite volume fraction was observed in the curves of models with the inhomogeneous ferrite phase. This result was expected due to the harder behavior of the ferrite phase in the higher martensite volume fraction.

3.6. The effect of martensite grain size

The effect of the martensite grain size on yield stress is shown in Figs. 19 and 20 for different martensite volume fractions. As shown, while martensite grain size had no effect on yield stress when ferrite phase was considered homogeneous, a significant difference was observed in the magnitude of the stresses of various grain sizes when ferrite phase inhomogeneity was considered. The mentioned result for models with the homogeneous ferrite phase was expected since the ferrite and martensite mechanical behaviors did not depend on grain size in these models. When ferrite phase inhomogeneity was considered, the average distance of the ferrite phase points from the FMBs was changed by changing martensite grain size; therefore, we could conclude that the mechanical properties of the ferrite phase were dependent on the martensite grain size in these models. By comparing with the experimental results [1,12,37], which showed martensite grain size dependency of DP steels, it could be concluded that considering the effects of FMB would lead to the better estimation of the grain size dependency. Fig. 21 compares the results of models with the homogeneous and inhomogeneous ferrite phase for various martensite grain sizes. The shear bands for the largest martensite islands were more

intense and thicker. The maximum strain was also increased with the martensite grain size, showing more strain localization in larger martensite grain sizes. However, considering the ferrite phase inhomogeneity had a slight effect on the predicted strain distribution in comparison with the macro stress.

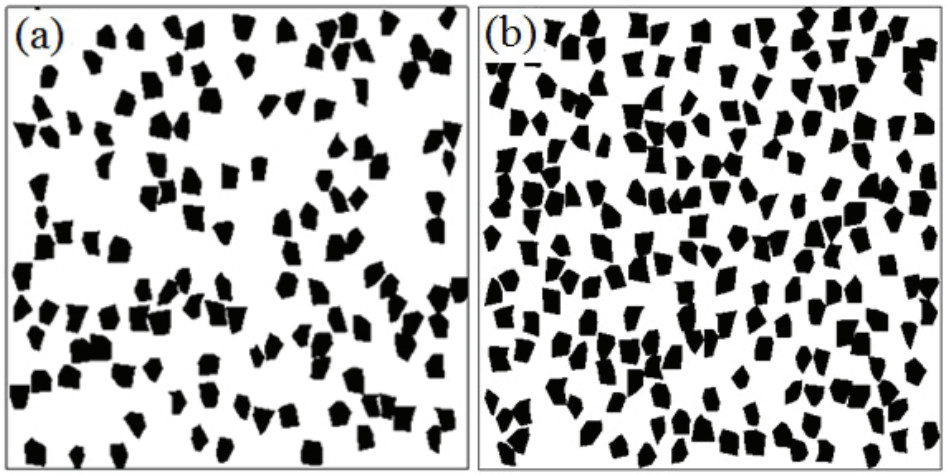

Fig. 17. Random created UC models with the martensite grain size of 2μm and the martensite volume fraction of (a) 20 percent, and (b) 30 percent.

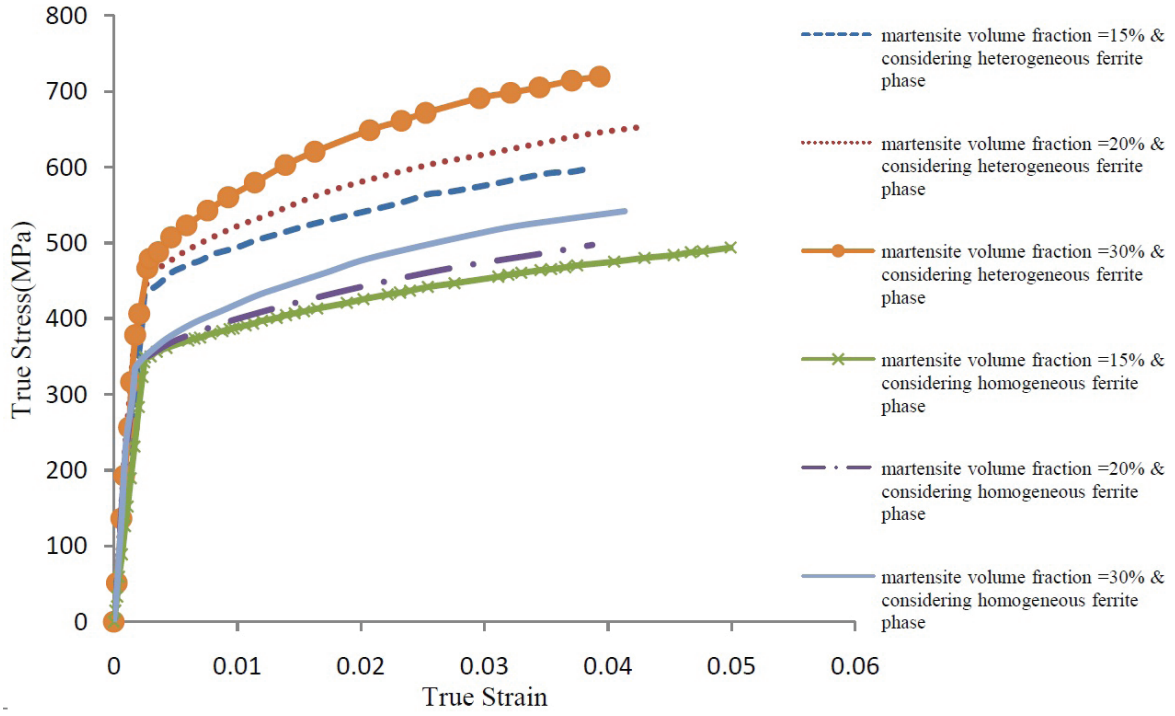

Fig. 18. The calculated macro stress-strain curve for different martensite volume fractions.

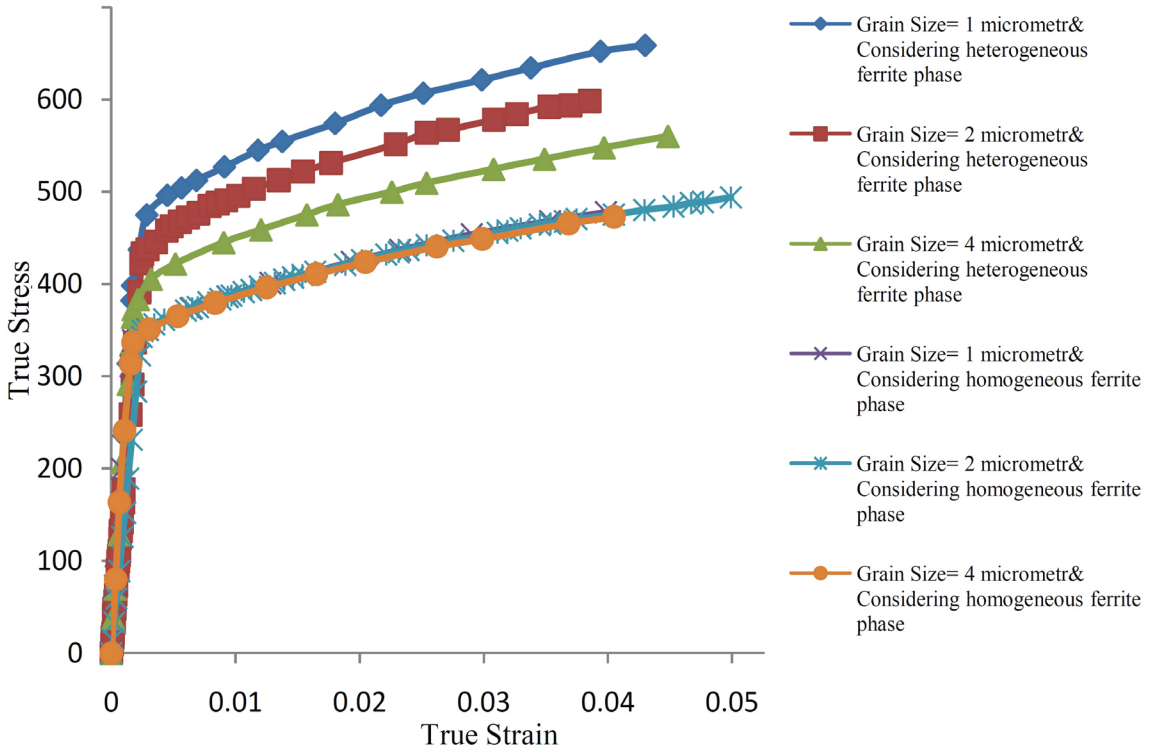

Fig. 19. The calculated macro stress-strain curve of UC with 15 percent martensite volume fractions and different martensite grain sizes.

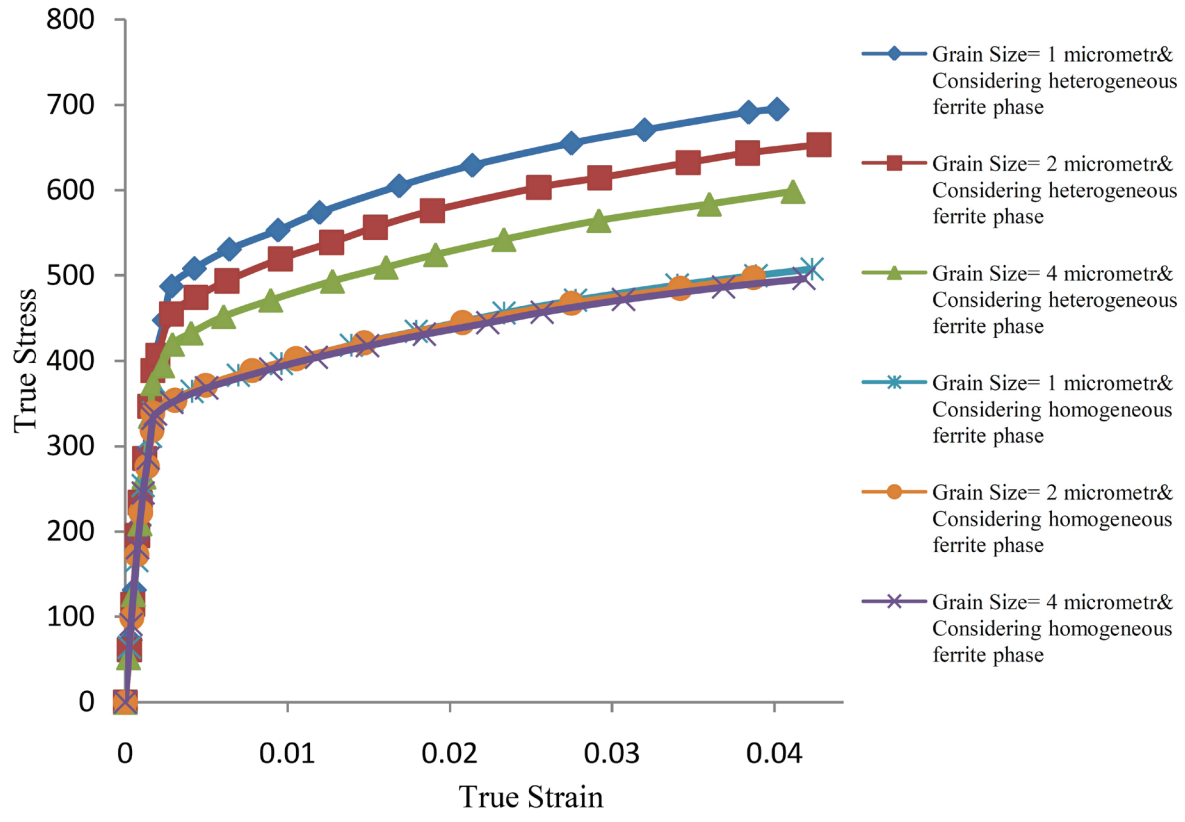

Fig. 20. The calculated macro stress-strain curve of UC with 20 percent martensite volume fraction and different martensite grain sizes.

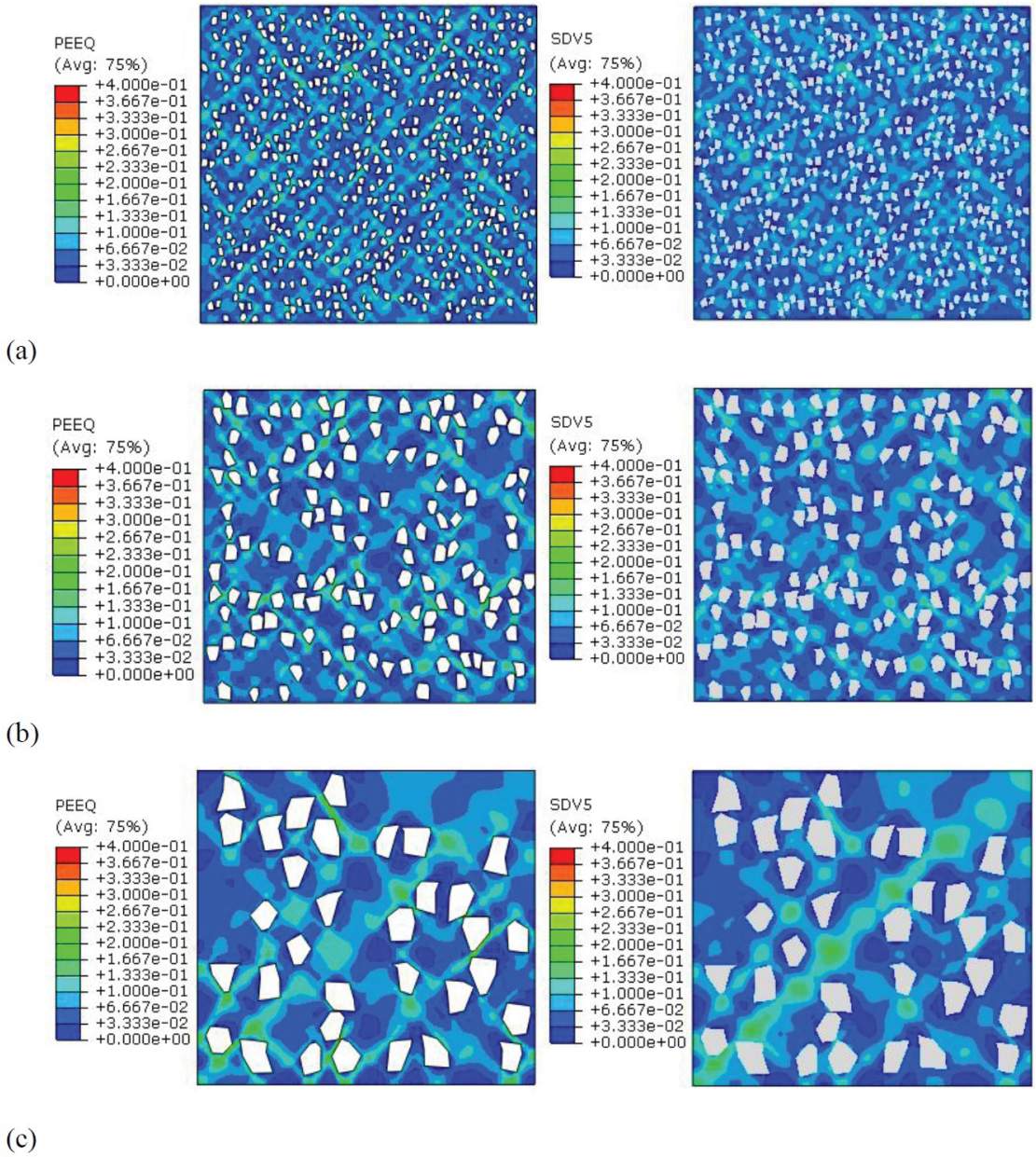

Fig. 21. The predicted effective plastic strain for UC model with 20% martensite volume fraction after 5% nominal strain, without (left) and with (right) FMB effect, and martensite grain size of (a)1μm, (b) 2μm and (c) 4μm.

5. Conclusions

In this paper, a method was proposed to consider ferrite phase inhomogeneity in the finite element modeling of DP steel microstructure. In this method, mechanical properties of each material point were considered as a continuous function of the distance from FMBs for the first time. It was observed that considering this inhomogeneity and comparing it to a homogeneous model led to:

I. better prediction of the macro stress-strain curve
II. better prediction of the formation of shear bands in simulations
III. different distributions of stress, showing a higher stress in phases' interfaces
IV. better prediction of martensite grain size dependency and
V. stronger martensite volume fraction dependency

Overall, these results showed the crucial role of the ferrite phase inhomogeneity in the damage prediction of DP steels. This is to be further investigated in authors' future works.

The current models did not use constitutive equations that would consider the directed behavior of crystals like crystal plasticity. Unfortunately, crystalline direction in the experimental measuremen were also ignored. This point should be investigated

both experimentally and numerically to obtain more insight into ferrite inhomogeneity effects. Moreover, the modeling can be reconstructed in the three-dimensional space to investigate the effects of plane strain assumption on the stress-strain curve and shear band formation.

References

[1] J. Kadkhodapour, S. Schmauder, D. Raabe, S. Ziaei-Rad, U. Weber, M. Calcagnotto: Acta. Mater., 59(2011), 4387.
[2] J. Kadkhodapour, B. Anbarlooie, H. Hosseini-Toudeshky, S.Schmauder: Comput. Mater. Sci., 94(2014), 106.
[3] F. Al-Abbasi and J. Nemes: Int. J. Solids. Struct., 40(2003), 3379.
[4] F. Al-Abbasi and J. Nemes: Int. J. Mech. Sci., 45(2003), 1449.
[5] F. Al-Abbasi, J. Nemes: Comput. Mater. Sci., 39(2007), 402.
[6] K. S. Choi, W. N. Liu, X. Sun, MA. Khaleel: Metall. Mater. Trans. A., 40(2009), 796.
[7] K. S. Choi, W. N. Liu, X. Sun, MA. Khaleel, J. Fekete: J. Eng. Mater. Technol. 131(2009), 412.
[8] X. Sun, K.S. Choi, W. N. Liu, MA. Khaleel: Int. J. Plast., 25(2009), 1888.
[9] X. Sun, K.S. Choi, A. Soulami, W. N. Liu, MA. Khaleel: Mater. Sci. Eng. A., 526(2009), 140.
[10] A. Ramazani, M. Abbasi, U. Prahl, W. Bleck: Comput. Mater. Sci., 64(2012), 101.
[11] A. Ramazani, K. Mukherjee, U. Prahl, W. Bleck: Comput. Mater. Sci., 52(2012), 46.
[12] A. Ramazani, K. Mukherjee, U.,Prahl, W. Bleck: Metall. Mater. Trans. A., 43(2012), 3850.
[13] A. Ramazani, K. Mukherjee, H. Quade, U.,Prahl, W. Bleck: Mater. Sci. Eng. A., 560 (2013)129.
[14] A. Ramazani, K. Mukherjee, A. Schwedt, P. Goravanchi, U.Prahl, W. Bleck: Int. J. Plast., 43(2013), 128.
[15] A. Ramazani, P. Pinard, S. Richter, A. Schwedt, U. Prahl: Comput. Mater. Sci., 80(2013), 134.
[16] K. Alharbi, H. Ghadbeigi, P. Efthymiadis, M. Zanganeh, S. Celotto, R. Dashwood and C. Pinna: Modell. Simul. Mater. Sci. Eng., 23(2015), 17.
[17] A. Srivastava, A. Bower, Jr. L. G. Hector, J. E. Carsley, L. Zhang and F. Abu-Farha: Modell. Simul. Mater. Sci. Eng., 24(2016).
[18] D. D. Tjahjanto, P. Eisenlohr and F. Roters, Modell. Simul: Mater. Sci. Eng., 23(2015).
[19] S-H. Choi, E-Y. Kim, W. Woo, S. Han, J. Kwak: Int. J. Plast., 45(2013), 85.
[20] S. Katani, S. Ziaei-Rad, N. Nouri, N. Saeidi, J. Kadkhodapour, N. Torabian, Metallography, Microstructure, and Analysis. 2(2013)156.
[21] JH. Kim, M-G. Lee, D. Kim, DK. Matlock, R. Wagoner: Mater. Sci. Eng. A., 527(2010), 7353.
[22] M. Marvi-Mashhadi, M. Mazinani, A. Rezaee-Bazzaz: Comput. Mater. Sci., 65(2012), 197.
[23] SK. Paul, A. Kumar: Comput. Mater. Sci., 63(2012), 66.
[24] S. Sodjit, V. Uthaisangsuk: Mater. Des., 41(2012), 370.
[25] N. Vajragupta, V. Uthaisangsuk, B. Schmaling, S. Münstermann, A. Hartmaier, W. Bleck: Comput. Mater. Sci., 54(2012), 271.
[26] H. Hosseini-Toudeshky, B. Anbarlooie, J. Kadkhodapour: Mater. Des., 68(2015), 167.
[27] T. Sirinakorn, S. Wongwises, V. Uthaisangsuk: Mater. Des., 64(2014), 729.
[28] NH. Abid, RK. A. Al-Rub, A. N. Palazotto, Comput: Mater. Sci., 103(2015), 20.
[29] M. Azuma, S. Goutianos, N. Hansen, G. Winther, X. Huang: Mater. Sci. Tech., 28(2012), 1092.
[30] M. Schellekens, Microstructural modeling of dual phase steel. Master Thesis. Department of Mechanical Engineering Eindhoven University of Technology, Eindhoven, (2010).
[31] JT. Busby, MC. Hash, GS. Was: J. Nucl. Mater., 336(2005), 267.
[32] M. Gaško, G. Rosenberg: J. Mater. Eng., (MEMI), 18(2011),155.
[33] LF. Ramos, DK. Matlock, G. Krauss: Metall. Mater. Trans. A., 10(1979), 259.
[34] A. Marder, Metal. Trans. A., 13(1982), 85.
[35] A. Bag, K. Ray, E. Dwarakadasa, Metall. Mater. Trans. A., 30(1999), 1193.
[36] M. Mazinani, W. Poole, Metall. Mater. Trans. A., 38(2007), 328.
[37] Z. Jiang, Z. Guan, J. Lian, Mater. Sci. Eng. A., 190(1995), 55.